 doi:10.20944/preprints201911.0012.v2

Article

Monitoring the Interfacial Polymerization of Piperazine and Trimesoyl Chloride with Hydrophilic Interlayer or Macromolecular Additive by in-situ FT-IR Spectroscopy

Xi Yang [1]*

[1] Department of Polymer Science & Engineering, Zhejiang University, China; xkyang@zju.edu.cn

* Correspondence: xkyang@zju.edu.cn; Tel.: +86-187-5810-1644

Abstract: The interfacial polymerization (IP) of piperazine (PIP) and trimesoyl chloride (TMC) has been extensively utilized to synthesize the nanofiltration (NF) membrane. However, it is still a huge challenge to monitor the IP reaction, because of the fast reaction rate and the formed ultra-thin film. Herein, two effective strategies are applied to reduce the IP reaction rate: (1) the introduction of hydrophilic interlayers between the porous substrate and the formed polyamide layer; (2) the addition of macromolecular additives in the aqueous solution of PIP. As a result, in-situ FT-IR spectroscopy was firstly used to monitor the IP reaction of PIP/TMC reaction system, with hydrophilic interlayers or macromolecular additives. Moreover, we study the formed polyamide layer growth on the substrate, in a real-time manner. The in-situ FT-IR experimental results confirm that the IP reaction rates are effectively suppressed and the formed polyamide thickness reduces from 138±24 nm to 46±2 nm. Furthermore, the optimized NF membrane with excellent performance are consequently obtained, which include the boosted water permeation flux about 141~238 (L·m^2·h/MPa) and superior salt rejection of Na_2SO_4 > 98.4%.

Keywords: interfacial polymerization; in-situ FT-IR spectroscopy; thin-film composite membrane; nanofiltration membrane

1. Introduction

The interfacial polymerization (IP) has been widely employed to fabricate the polyamide-based membranes with a typical thin-film composite structure, which include polyamide layer, ultrafiltration support and non-woven fabric. These membranes have been extensively used in reverse osmosis (RO) [1,2], nanofiltration (NF) [3], and forward osmosis (FO) [4,5]. The IP usually takes place at the interface of two immiscible solvents, dissolving the two kind of reactive monomers include diamine monomer and acid chloride monomer [6]. The acid chloride monomer dissolves in the organic phase, while the diamine monomer is soluble both in the aqueous phase and the organic phase. As a result, the diamine monomer is able to diffuse into the organic phase and subsequently react with acid chloride monomer at the interface near the organic phase side, and then immediately form the polyamide ultra-thin film at the interface [7]. As a consequent, the IP reaction has been successfully utilized to synthesize the ultra-thin and dense polyamide layer on top surface of a porous substrate, which serves both as the storage place of the diamine monomer, and as the support of formed ultra-thin polyamide film [8,9].

The IP reaction usually has a rapid reaction rate about 10^4 L/mol·s, and the thickness of the formed ultra-thin film is normally less than 100 nm. Therefore, it is a huge challenge to monitor the IP reaction in a real time manner, and to investigate the IP reaction kinetics directly on the porous substrates [10]. To the best of our knowledge, few methods have been developed to study the IP

Preprints (www.preprints.org) | NOT PEER-REVIEWED | Posted: 6 November 2019 doi:10.20944/preprints201911.0012.v2

reaction, where the polyamide film was formed at the free water/oil interface. It is possible for one to terminate the IP reaction at different times, including determining the film mass [11], measuring the film thickness [12], and/or analyzing the reactant concentration [13-15]. Furthermore, the polyamide film formation at the free water/oil interface was also observed by measuring the suspended drop interfacial tension [16], light reflection [16], and diffusion reflectance spectra [17]. Matthews et al. used Rutherford backscattering spectrometry (RBS) to study the polyamide growth dynamics, and established a relationship between the diffusion reflectance and the polyamide layer thickness [17]. Recently, Nowbahar et al. applied the microfluidic interferometry to measure the IP reaction kinetics of m-phenylenediamine (MPD)/trimesoyl chloride (TMC) reaction system [10]. Although these techniques can be used to roughly estimate the IP reaction, they are still limited to detect the IP reaction at the free water/oil interface, instead of directly on the porous substrate. Therefore, it is of great significance to develop effective strategies for monitoring the IP reaction, which takes place on the substrate in a real-time manner.

Herein, we report the in-situ Fourier transform infrared (FT-IR) spectroscopy as an effective instrument to monitor the IP reaction and the polyamide film growth on the porous substrate in real-time. In-situ FT-IR spectroscopy is a powerful and well-established tool to investigate the reaction taking place at the solid/liquid interface [18,19], and to provide the real-time information about the reaction, such as mechanism and kinetics [20,21]. For example, Han et al. used a self-made FT-IR sample cell to monitor the photo-polymerization of alicyclic methacrylate hydrogel for the controlled drug release [22]. Zimudzi et al. analyzed the Nafion film thickness [23], and quantified the carboxylic acid concentration in the polyamide-based membrane [24]. Moreover, it is reasonable to associate the absorbance intensity of characteristic band in the FT-IR spectra with the polyamide film thickness by the mathematical equations [25-28]. Additionally, Ren et al. used FT-IR microscopy for IP reaction of microporous polymer film formed in the aqueous/organic interface, for polyesterification by choosing the adequate phenol monomer [29]. Yang et al. reduced the IP reaction rate of piperazine (PIP) and trimesoyl chloride (TMC) reaction system to a certain extent, by introducing interlayers between the porous substrate and the polyamide layer [30-32]. Tan et al. added the macromolecular additives in the aqueous solution of PIP and obtained the Turing structure [33]. Furthermore, in-situ FT-IR spectroscopy is used to measure the IP reaction in real-time. The relationship between the IP reaction rate and the polyamide film thickness is successfully established, for laying a foundation to optimize the NF membrane performance. The fabricated NF membranes exhibit the boosted water permeation flux about 141~238 ($L \cdot m^2 \cdot h/MPa$) and superior salt rejection of Na_2SO_4 > 98.4%. These improved NF membrane performance are attributed to the reduced polyamide layer thickness and the remained high cross-linking degree of the internal structure of polyamide layer.

2. Materials and Methods

2.1. Materials

Polysulfone (PSf) ultrafiltration membranes with the molecular weight cut-off (MWCO) of 50 kDa were used as the porous substrates, and were purchased from Ande Membrane Separation Technology & Engineering Co., Ltd (USA). Dopamine hydrochloride (DA), tris (hydroxymethyl) aminomethane (Tris) and N,N-bis (2-hydroxyethyl) glycine (Bicine) were obtained from Sigma-Aldrich (USA). Polyethyleneimine (PEI, M_w~600 Da), tannic acid (TA), polyethyleneglycol (PEG, M_w=20,000), polyvinylpyrrolidone (PVP, K23-27, M_w~24,000), polyvinyl alcohol (PVA 1788, M_w 75,000-80,000, 87-89% hydrolyzed) and piperazine (PIP) were received from Aladdin Chemical Co., Ltd (China). Trimesoyl chloride (TMC) was procured from Qingdao Benzo Chemistry Co., Ltd (China). 2-Methylimidazole (Hmim) was purchased from Tokyo Chemical Industry Co., Ltd (Japan). Other chemicals, including $Zn(NO_3)_2 \cdot 6H_2O$, n-hexane, ethanol and inorganic salts (Na_2SO_4, $MgSO_4$, $MgCl_2$, $CaCl_2$, and NaCl) were bought from Sinopharm Chemical Reagent Co., Ltd (China). Ultrapure water consumed in the experiments was directly generated from a lab water purification system (HYP-QX, China).

Preprints (www.preprints.org) | NOT PEER-REVIEWED | Posted: 6 November 2019 doi:10.20944/preprints201911.0012.v2

2.2 Fabrication of interlayers on the porous substrate

The porous substrates were cut into circular shape with a diameter of 47 mm and rinsed in deionized (DI) water and ethanol overnight. Various interlayers were fabricated on the porous substrate includes polydopamine (PDA)/polyethyleneimine (PEI), tannic acid (TA)/polyethyleneimine (PEI) and zeolitic imidazolate framework-8 (ZIF-8)/polyethyleneimine (PEI), respectively.

The PDA/PEI interlayer was constructed on the porous substrate, according to the reported literature. DA and PEI were dissolved in Tris-buffer (50 mM, pH = 8.5) at a mass ratio of 1:1, with a concentration of 2.0 mg/mL [30]. The porous substrate was immersed in the freshly prepared DA/PEI solution for 1 h. After that, the PDA/PEI modified substrate was washed thoroughly by DI water and dried at room temperature for 1 h.

The TA/PEI interlayer was fabricated on the porous substrate via Michael addition or Schiff base reaction between the amino groups and quinone groups [31]. TA (2.0 mg/mL) was dissolved in a Bicine buffer solution (pH=7.8), then PEI (2.0 mg/mL) was added in the solution. The substrate was immersed in the freshly prepared TA/PEI solution for 1 h, followed by washing procedure with DI water and drying at room temperature for 1 h of the TA/PEI modified substrate.

The ZIF-8/PEI interlayer was constructed on the porous substrate with the following steps [34,35]. The porous substrate was immersed in an equal volume of 0.1 mol/L Zn $(NO_3)_2$ aqueous solution and 0.4 wt% PEI aqueous solution for 0.5 h, at 25±2 °C. Next, the substrate was rinsed with DI water to remove the excess residual PEI. Then the porous substrate was immersed in 0.2 mol/L Hmim in n-hexane solution, which reacted with Zn^{2+} for 0.5 h. The as-prepared ZIF-8/PEI modified substrate was rinsed with DI water and dried at room temperature for further usage.

2.3 IP on the substrates with modified interlayers

The porous substrates modified with as-formed interlayers were upper-side immersed in 10 mL aqueous solution of 2.0 g/L PIP for 10 min, ensuring the complete adsorption and infiltration of diamine solution on the interlayer surfaces and the substrate internal pores. A rubber roller was gently used to dry the excess PIP solution on the top surface. Then, 10 mL of TMC solution with the concentration of 2.0 g/L in n-hexane was carefully poured on the substrates. Therefore, IP reaction was then consequently carried out for about 100 seconds of the IP reaction time, to form the ultra-thin polyamide layers on top surfaces of the porous substrates.

2.4 IP on the substrates with macromolecular additives

Macromolecular additives of PEG, PVP and PVA were added respectively, in the aqueous solution of PIP. The aqueous solutions were prepared by mixing 1.5 g/L of macromolecular additive evenly with 2 g/L of PIP. The aqueous solutions were stirred at 25±2 °C for 1 h and rested for 30 min to be uniformly mixed and to eliminate air bubbles. Then the IP reaction was then conducted on the porous substrates. The resulted membranes were post-treated in an oven for 30 min at 60 °C, in order to further solidify and stabilize the formed polyamide layer.

2.5 Measuring IP reaction by in-situ FT-IR spectroscopy

Polyamide formation on the porous substrates were measured by in-situ FT-IR spectroscopy (React 15, Mettler Toledo, Switzerland), with the scan range between 4000-650 cm^{-1}, the maximum resolution of 4 cm^{-1} and the minimum detection time interval of 15 seconds. During the detection process, one sample of the porous substrate was fixed in a home-made reactor, to ensure the upper-side contacting with the monomer solutions of PIP and TMC. Firstly, 10 mL of PIP solution (2.0 g/L) was poured onto the substrate surface for 10 min. It was then poured off the PIP solution thoroughly and wiped off by filter paper to remove the excess PIP solution on the surface. An optic probe was tightly contacted with the middle area of the substrate surface. Then, 10 mL of TMC solution (2.0 g/L) was poured on the substrate surface, for conducting the IP reaction. Data collection was instantaneously

Preprints (www.preprints.org) | NOT PEER-REVIEWED | Posted: 6 November 2019 doi:10.20944/preprints201911.0012.v2

began by in-situ FT-IR spectroscopy monitoring process. Subsequently, the FT-IR absorbance intensity was acquired and calculated from the polyamide film formation, as a function of IP reaction time.

2.6 Other characterizations

Surface morphologies were observed by field emission scanning electron microscopy (FESEM, Hitachi, SU-8010, Japan) for the porous substrates and the formed polyamide layer. Topographies and surface roughness were measured by atomic force microscopy (AFM, MultiMode, Vecco, USA) in the tapping mode. Transmission electron microscopy (TEM, Hitachi 7650, Japan) was applied to observe the cross-sectional morphologies and to measure the thickness of polyamide layer. The samples were embedded in LR white resin (London Resin Company, Reading, UK), cut by ultramicrotome (Leica Microsystems, Wetzlar, Germany) and then mounted to copper grids. Chemical structures were analyzed by attenuated total reflectance Fourier transform infrared spectrometry (ATR/FT-IR, Nicolet 6700, USA) and X-ray photoelectron spectrometry (XPS, Thermo Scientific, USA), respectively. Surface hydrophilicity was measured by a contact angle measurement system (Surface-Meter, OCA 200, China). The surface zeta potential was evaluated by an electro kinetic analyzer (SurPASS Anton Paar, GmbH, Austria).

2.7 NF membrane performance evaluation

NF membrane performance of the as-formed membranes were evaluated by a laboratory scale cross-flow flat module. The effective filtration area was 7.07 cm^2 and the cross-flow rate was 30 L/h under the operation pressure of 0.6 MPa at room temperature. Various inorganic salts, including Na_2SO_4, $MgSO_4$, $MgCl_2$, $CaCl_2$, and NaCl, were dissolved in DI water at a concentration of 1000 mg/L to prepare the feed solutions. The water permeation flux (J_w, $L/m^2 \cdot h$) and the salt rejection (R, %) were calculated by the following equations:

$$J_w = \frac{V}{A \cdot t} \quad (1)$$

where V (L), A (m^2), and t (h) represent the filtered water volume, the effective membrane area, and the permeation time, respectively.

$$R = \left(1 - \frac{C_p}{C_f}\right) \times 100\% \quad (2)$$

where C_p and C_f (mg/L) are the feed and permeated solution concentrations, determined by an electrical conductivity meter (Mettler Toledo, FE30, China) for average value as a result of three times measurements.

3. Results and Discussion

Typical IP reaction is usually finished in 0.5~2.0 min, because of the fast and uncontrollable IP reaction. In this work, hydrophilic interlayers and macromolecular additives are used, respectively, to reduce the IP reaction rate, for in-situ FT-IR spectroscopy analyzing (as schematically shown in Figure 1). In addition, ATR/FT-IR spectra validate the formation of interlayers including PDA/PEI, TA/PEI and ZIF-8/PEI on the porous substrates (Figure S1). As a result, the formed interlayers have reasonably changed the surface morphology, surface hydrophilicity, and surface charge of the porous substrates (Figure S2-S3).

Figure 2 and Figure 3 show the in-situ FT-IR spectra monitoring the IP reaction on the porous substrates of C=O stretching vibration at 1640 cm^{-1}. The absorbance intensities are also shown in the Figure S4-S5, as an indicator of the polyamide formation process. It is exhibited that the IP reaction is ideally considered as three different stages, in consistence with the reported literature [36,37]. The first stage of the incipient dense film formation, second stage of the slowed-down reaction and then

Preprints (www.preprints.org) | NOT PEER-REVIEWED | Posted: 6 November 2019 doi:10.20944/preprints201911.0012.v2

finally reached the "self-limited" film growth. Figure 2 shows that the in-situ FT-IR spectra monitor the IP reaction on the nascent PSf porous substrate, which nicely complies with the traditional growth principle. However in other cases, the IP reactions are obviously repressed, in the condition of the introduction with hydrophilic interlayers and/or macromolecular additives. The reason for the repression phenomena could be possibly attributed to the slowed-down PIP diffusion rates, which are studied and acquired from the ultraviolet spectroscopy (UV-vis) analyses, as shown in Figure S6. As a result, the measured PIP diffusion rates are commendably in accordance with the decreased diffusion co-efficient reported in the literature [33], which reduces from about 10^{-5} cm^2/s to 10^{-6} cm^2/s, as shown in Table S1.

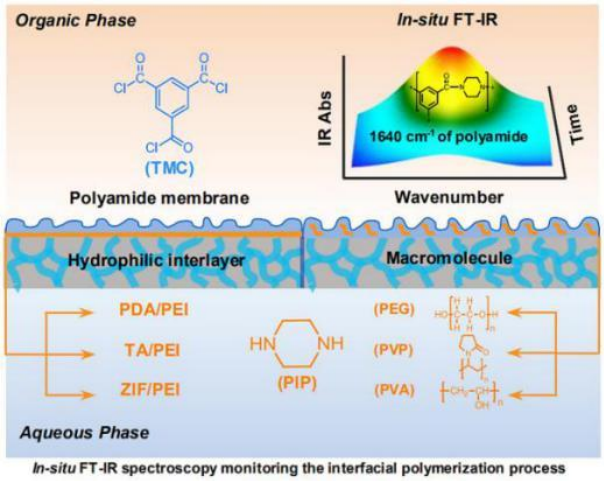

Figure 1. In-situ FT-IR spectroscopy monitoring the IP reaction of PIP and TMC by the introduction of hydrophilic interlayers and macromolecular additives in the aqueous solution of PIP.

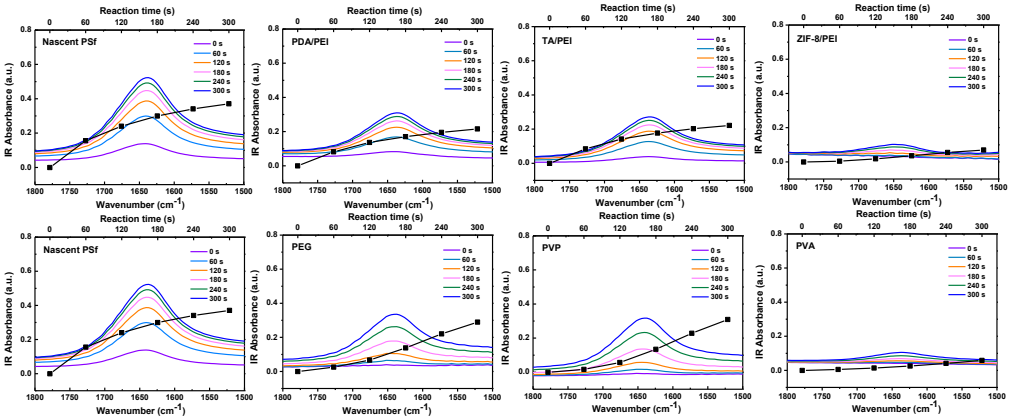

Figure 2. The in-situ FT-IR spectra and absorbance intensities growth of polyamide formation process on porous substrate, which are characterized by the C=O stretching vibration at 1640 cm^{-1}.

Preprints (www.preprints.org) | NOT PEER-REVIEWED | Posted: 6 November 2019 doi:10.20944/preprints201911.0012.v2

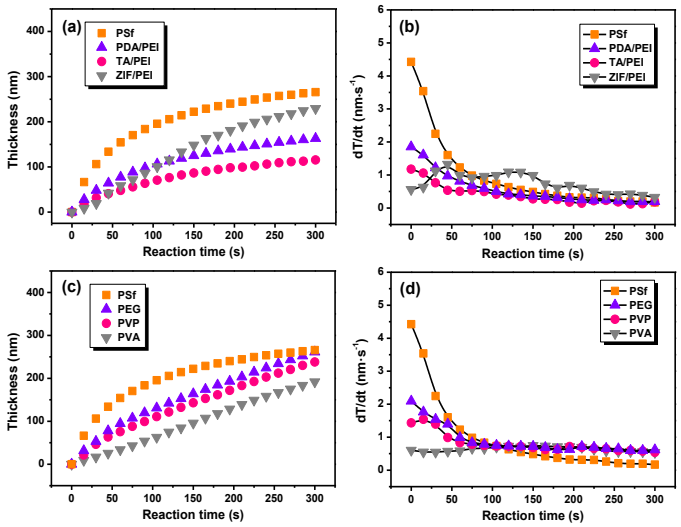

Figure 3. The growth of polyamide layer thickness and the correspondingly calculated layer thickness growth rate, as a function of IP reaction time including (a and b) IP reaction taking place on the porous substrates, with various modified interlayers (c and d) the doped polyamide layer with the macromolecular additives in the aqueous solution of PIP.

Furthermore, the reduced IP reaction rate could also arise from the combination results of enhanced storage ability of PIP in the interlayers, and the enhanced interactions between the PIP and interlayers (Table S2 and Figure S7). In detail, the adhesive PDA/PEI and TA/PEI interlayers impede the IP reaction rate and maintain the similar growth tendency, compared with the IP reaction on the nascent PSf substrate. Additionally, polyamide growth on the ZIF-8/PEI interlayer obeys the approximately painful and linear propensity. The reason is that the ZIF-8/PEI is a high-porosity and inorganic interlayer, which restores and reduces PIP diffusion greatly. As for the doped polyamide layer with the macromolecular additives, polyamide growth are considerably repressed, because of the low flow viscosity of macromolecular additives and their strong hydrogen-bonding interactions with the PIP monomer (as shown in the Figure S8-S9).

It is still a huge challenge to measure the polyamide layer thickness, which in-situ formed on the porous substrate. Previously, various methods were used to deal with this issue, including reducing the IP reaction rate [11], and/or stopping the IP reaction at various times and then determing the film mass or thickness [12]. The mathematical model predicts that the polyamide film thickness is increasing with the IP reaction time as $t^{1/2}$, which is reported in the literatures [36,37]. In our study, the in-situ FT-IR absorbance intensity is related with the polyamide layer thickness. Figure 3 shows the growth rate of polyamide thickness, as a function of the IP reaction time. It can be seen that the IP reaction taking place on the nascent PSf substrate holds the fastest film thickness increasing rate. In addition, the layer thickness of polyamide with the IP reaction time can be fitted as $X = 24.8\ t^{1/2}$, where X (nm) is polyamide thickness and t (s) is the IP reaction time (Table S3). Furthermore, the growth of polyamide layers thickness are mathematically described as $X = 7.3\ t^{1/2}$, $4.0\ t^{1/2}$ and $0.6\ t$ on the various substrates modified with PDA/PEI, TA/PEI, and ZIF-8 interlayers, respectively (as shown in Figure 3a-3b and Table S3). At the same time, when the macromolecular additives are added in the aqueous solution of PIP (Figure 3c-3d and Table S3), the growth of polyamide thickness corresponds to $X = 5.4\ t^{2/3}$, $3.3\ t^{2/3}$ and $0.5\ t$, respectively, which imply the repressed IP reaction rate by the introduction of macromolecular additives in the aqueous solution of PIP.

In the aim of confirming the accuracy and reliability of in-situ FT-IR spectroscopy method for the determination of the thickness of polyamide layer, the TEM technique is employed, as shown in Figure 4 and Figure S10. Figure 4 exhibits that the thickness of polyamide layers decrease noticeably, by the introduction of interlayers and/or macromolecular additives. The ascertained thickness of polyamide layers obtained from the TEM images are at the sequence of 138±24 nm (PSf) > 95±7 nm

Preprints (www.preprints.org) | NOT PEER-REVIEWED | Posted: 6 November 2019 doi:10.20944/preprints201911.0012.v2

(PEG) > 84±17 nm (PVP) > 76±19 nm (PVA) > 71±3 nm (PDA/PEI) > 60±6 nm (ZIF-8/PEI) > 46±2 nm (TA/PEI). Furthermore, the as-formed polyamide layer surface morphologies and the roughness are observed and evaluated by the FESEM images (Figure S11) and the AFM images (Figure S12 and Table S4). The obtained results shown that the polyamide surface morphologies maintain the "nodular" structures on the nascent PSf substrate and the substrates modified with various interlayers. Furthermore, with the ever-increasing ability of PVA > PVP > PEG to retard the PIP diffusion rate, the doped polyamide layers with macromolecular additives could generated the Turing structure as reported in the literature [33].

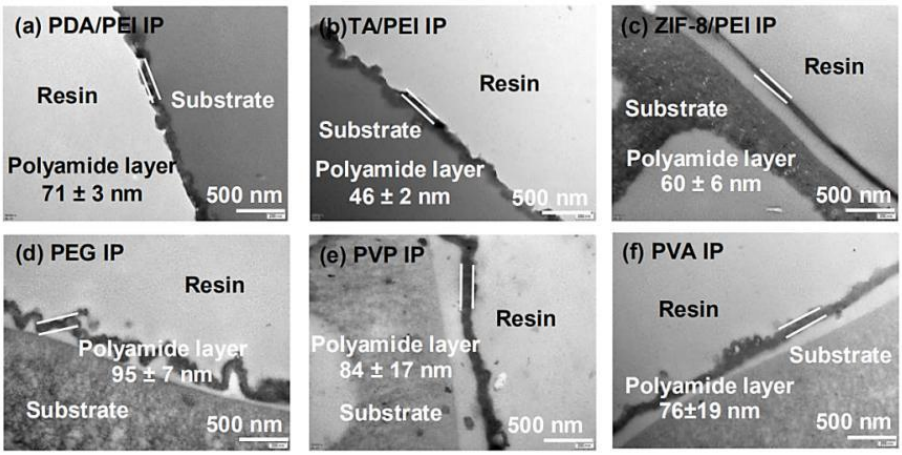

Figure 4. TEM observation of thickness of the formed polyamide layer on the (a-c) porous substrates with various modified interlayers and (d-f) the doped polyamide layer with the macromolecular additives in the aqueous solution of PIP.

Moreover, the XPS analyses are used to investigate the elemental content near the polyamide layer surface (shown in Table S5). In regard of the traditional formed polyamide membrane on the nascent PSf substrate, polyamide layer retains the conventional "sandwich-structure", which means the densest part is in the middle of the polyamide layer structure [36,37]. In contrast, compared with the traditional polyamide structure, the polyamide layers formed on the substrates modified with hydrophilic interlayers lead to the looser top structures, including the higher O/N ratio and lower cross-linking degree (shown in Table S5). Nevertheless, for doped polyamide layers with the macromolecular additives added in the aqueous PIP solution, the polyamide layer top structures are comparatively denser, including the lower O/N ratio and higher cross-linking degree (shown in Table S5) [38].

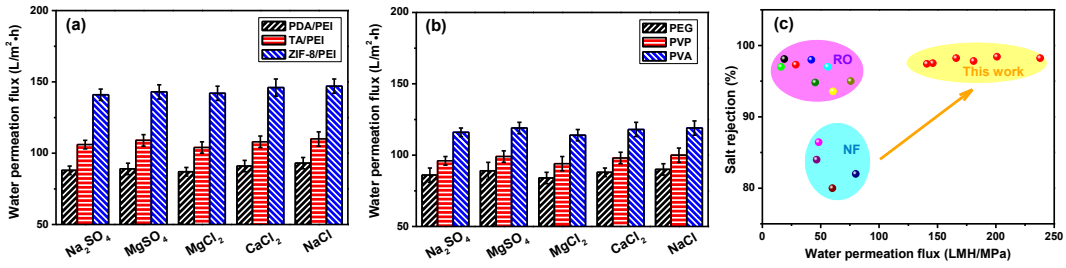

Figure 5. Water permeation flux of the as-prepared NF membranes with (a) the hydrophilic modified interlayers on the porous substrates or (b) the addition of macromolecular additives in the aqueous PIP solution (test conditions: inorganic salts concentration = 1000 mg/L, pH = 6.0, 25 °C, applied pressure = 0.6 MPa and cross-flow rate = 30 L/h) (c) the comparison of the NF performance with other thin-film composite membranes in the reported literature [39].

 doi:10.20944/preprints201911.0012.v2

NF performances of the as-prepared polyamide membranes are evaluated by a laboratory cross-flow equipment. The membranes surface hydrophilicity are significantly improved by the introduction of interlayers and/or addition of macromolecular additives in the aqueous PIP solution. Besides, polyamide membranes surface charge are evaluated by the zeta potential analyzer (shown in Table S6). The results of their surface charges indicate that NF membranes with the hydrophilic modified interlayers have the higher surface charges, compared with the doped polyamide membranes with macromolecular additives.

It is noticeable that the NF performances including the water permeation flux and inorganic salts rejection rate are usually the synergistic results of the polyamide layer thickness and their internal cross-linking degree. In the aim of obtaining the high membrane water permeation flux, the polyamide layer thickness is expected to be as thin as possible. Otherwise, for achieving the high inorganic salts rejection rate, the membrane internal high cross-linking degree is necessarily required. In our experiments, after the introduction of hydrophilic interlayers and/or adding of the macromolecular additives in the aqueous PIP solution, water permeation flux enhancements are noteworthy, which is at the order of ZIF-8/PEI > TA/PEI > PDA/PEI with the hydrophilic interlayers on the modified porous substrates, and PVA > PVP > PEG for the doped polyamide membranes with macromolecular additives (as shown in Figure 5a-5b, respectively).

Furthermore, inorganic salts rejection of these NF membranes are presented at the order of Na_2SO_4 > $MgSO_4$ > $MgCl_2$ > $CaCl_2$ > NaCl (Table S7), which is in accordance with the typical NF membranes carried with the surface negative charges. In particular, the high rejections of $MgCl_2$ and $CaCl_2$ for these doped polyamide membranes with macromolecular additives could be attributed to the compactly packing of the macromolecular additives in the polyamide layer structures. By taking into account the combination of size sieving and Donnan exclusion effects, the hydrated radius of ions is at the order of Mg^{2+} (0.428 nm) > Ca^{2+} (0.412 nm) > Na^{+} (0.358 nm), thus the resulted rejection of NF membranes is at the sequence of $MgCl_2$ > $CaCl_2$ > NaCl [40,41]. What's more, the electrostatic interaction between SO_4^{2-} and the polyamide negative surface is stronger than Cl^{-}, leading to the high rejections of Na_2SO_4 and $MgSO_4$ (exceed above 97.2%). In summary, the as-prepared NF membranes provide the great chance to break out the "trade-off" behavior of the traditional polyamide membranes, showing the high water permeation flux, and maintaining the superior inorganic salts rejection rate (as shown in Figure 5c) [39].

5. Conclusions

To sum up, in-situ FT-IR spectroscopy is employed to measure the IP reaction on the porous substrate. Our results validate the "depressed-effect" of both the introduced interlayers and macromolecular additives in the PIP solution during the IP reaction process. Though the exact mechanism of the dissimilar growing types of IP reaction are still not cleared, the in-situ FT-IR spectroscopy has paved a new way for us to thoroughly comprehend the IP reaction mechanism. Furthermore, it could be utilized to tailor the superior performing thin-film composite membrane, and consequently surmount the notorious "trade-off" effect.

Supplementary Materials: Figure S1-S12 and Table S1-S7 are available online at www.mdpi.com/xxx/s1.

Acknowledgments: The author thanks the Prof. Zhi-Kang Xu, Prof. Guang-Peng Wu and Dr. Jing Yang in Department of Polymer Science & Engineering at Zhejiang University, for their help in the discussion regarding of the experimental design, results analysis and manuscript preparation.

Conflicts of Interest: The authors declare no conflict of interest.

References

1. Elimelech, M.; Phillip, W. A. The future of seawater desalination: energy, technology, and the environment. *Science* **2011**, *333*, 712–717.

2. Werber, J. R.; Osuji, C. O. Materials for next-generation desalination and water purification membranes. *Nat. Rev. Mater.* **2016**, *1*, 16018.

3. Lv, Y.; Du, Y. Polymer nanofiltration membranes via controlled surface/interface engineering. *Acta Polym. Sin.* **2017**, *12*, 1905–1914.

4. Giagnorio, M.; Ricceri, F. Desalination of brackish groundwater and reuse of wastewater by forward osmosis coupled with nanofiltration for draw solution recovery. *Water Res.* **2019**, *153*, 134–143.

5. Jin, L.; Wang, Z. Polyamide-crosslinked graphene oxide membrane for forward osmosis. *J. Memb. Sc*i. **2018**, *545*, 11–18.

6. Karan, S.; Jiang, Z. Sub–10 nm polyamide nanofilms with ultrafast solvent transport for molecular separation. *Science* **2015**, *348*, 1347–1351.

7. Freger, V. Nanoscale heterogeneity of polyamide membranes formed by interfacial polymerization. *Langmuir* **2003**, *19*, 4791–4797.

8. Zhang, X.; Lv, Y. Polyphenol coating as an interlayer for thin-film composite membranes with enhanced nanofiltration performance. *ACS Appl. Mater. Interfaces* **2016**, *8* , 32512–32519.

9. Wang, J.-J.; Yang, H.-C. Nanofiltration membranes with cellulose nanocrystals as an interlayer for unprecedented performance. *J. Mater. Chem. A* **2017**, *5*, 16289–16295.

10. Nowbahar, A.; Mansard, V. Measuring interfacial polymerization kinetics using microfluidic interferometry. *J. Am. Chem. Soc.* **2018**, *140*, 3173–3176.

11. Ji, J.; Dickson, J. M. Mathematical model for the formation of thin-film composite membranes by interfacial polymerization: porous and dense films. *Macromolecules* **2000**, *33*, 624–633.

12. Bouchemal, K.; Couenne, F. Polyamides nanocapsules: modeling and wall thickness estimation. *AIChE J.* **2006**, *52*, 2161–2170.

13. Wagh, S. J.; Dhumal, S. S. An experimental study of polyurea membrane formation by interfacial polycondensation. *J. Memb. Sci.* **2009**, *328*, 246–256.

14. Yadav, S. K.; Suresh, A. K. Microencapsulation in polyurea shell by interfacial polycondensation. *AIChE J.* **1990**, *36*, 431–438.

15. Behera, S.; Suresh, A. K. Kinetics of interfacial polycondensation reactions–development of a new method and its validation. *Polymer* **2017**, *127*, 28–44.

16. Chai, G.-Y.; Krantz, W. B. Formation and characterization of polyamide membranes via interfacial polymerization. *J. Memb. Sci.* **1994**, *93*, 175–192.

17. Matthews, T. D.; Yan, H. Growth dynamics of interfacially polymerized polyamide layers by diffuse reflectance spectroscopy and Rutherford backscattering spectrometry. *J. Memb. Sci.* **2013**, *429*, 71–80.

18. Mul, G.; Hamminga, G. M. Operando ATR-FTIR analysis of liquid-phase catalytic reactions: can heterogeneous catalysts be observed? *Vib. Spectrosc.* **2004**, *34*, 109–121.

19. Hind, A. R.; Bhargava, S. K. At the solid/liquid interface: FTIR/ATR–the tool of choice. *Adv. Colloid Interface Sci.* **2001**, *93*, 91–114.

20. Sawunyama, P.; Jiang, L. Photodecomposition of a Langmuir−Blodgett film of stearic acid on TiO_2 film observed by in situ atomic force microscopy and FT-IR. *J. Phys. Chem. B* **1997**, *101*, 11000–11003.

21. Andrew Chan, K. L.; Kazarian, S. G. FT-IR spectroscopic imaging of reactions in multiphase flow in microfluidic channels. *Anal. Chem.* **2012**, *84* , 4052–4056.

22. Han, J.; He, Y. Photopolymerization of alicyclic methacrylate hydrogels for controlled release. *Polym. Adv. Technol.* **2009**, *20*, 607–612.

23. Zimudzi, T. J.; Hickner, M. A. Signal enhanced FTIR analysis of alignment in Nafion thin films at SiO_2 and Au interfaces. *ACS Macro Lett.* **2016**, *5*, 83–87.

24. Zimudzi, T. J.; Feldman, K. E. Quantifying carboxylic acid concentration in model polyamide desalination membranes via Fourier transform infrared spectroscopy. *Macromolecules* **2018**, *51*, 6623–6629.

25. Singh, P. S.; Rao, A. P. Techniques for characterization of polyamide thin film composite membranes. *Desalination* **2011**, *282*, 78–86.

26. Ohta, K.; Iwamoto, R. Experimental proof of the relation between thickness of the probed surface layer and absorbance in FT-IR/ATR spectroscopy. *Appl. Spectrosc.* **1985**, *39*, 418–425.

27. Jin, Y.; Su, Z. Effects of polymerization conditions on hydrophilic groups in aromatic polyamide thin films. *J. Memb. Sci.* **2009**, *330*, 175–179.

28. Singh, P. S.; Joshi, S. V. Probing the structural variations of thin film composite RO membranes obtained by coating polyamide over polysulfone membranes of different pore dimensions. *J. Memb. Sci.* **2006**, *278*, 19–25.

29. Ren, D.; Yeo, J. I. N. Time-dependent FTIR microscopy for mechanism investigations and kinetic measurements in interfacial polymerisation: a microporous polymer film study. *Polym. Chem.* **2019**, *10*, 2769–2773.

30. Yang, X.; Du, Y. Nanofiltration membrane with a mussel-inspired interlayer for improved permeation performance. *Langmuir* **2017**, *33*, 2318–2324.

31. Yang, X. Controllable interfacial polymerization for nanofiltration membrane performance improvement by the polyphenol interlayer. *ACS Omega* **2019**, *4*,13824-13833.

32. Wu, X.; Li, Y. Adsorption-assisted interfacial polymerization toward ultrathin active layers for ultrafast organic permeation. *ACS Appl. Mater. Interfaces* **2018**, *10*, 10445–10453.

33. Tan, Z.; Chen, S. Polyamide membranes with nanoscale Turing structures for water purification. *Science* **2018**, *360*, 518–521.

34. Yang, L.; Wang, Z. Highly permeable zeolite imidazolate framework composite membranes fabricated via a chelation-assisted interfacial reaction. *J. Mater. Chem. A* **2017**, *5*, 15342–15355.

35. Yang, L.; Wang, Z. Zeolite imidazolate framework hybrid nanofiltration (NF) membranes with enhanced permselectivity for dye removal. *J. Memb. Sci.* **2017**, *532*, 76–86.

36. Freger, V.; Srebnik, S. Mathematical model of charge and density distributions in interfacial polymerization of thin films. *J. Appl. Polym. Sci.* **2003**, *88*, 1162–1169.

37. Freger, V. Kinetics of film formation by interfacial polycondensation. *Langmuir* **2005**, *21*, 1884–1894.

38. Kong, X.; Qiu, Z.-L. High permselectivity hyperbranched polyester/polyamide ultrathin films with nanoscale heterogeneity. *J. Mater. Chem. A* **2017**, *5*, 7876–7884.

39. Hu, R.; Zhang, R. Graphene oxide-in-polymer nanofiltration membranes with enhanced permeability by interfacial polymerization. *J. Memb. Sci.* **2018**, *564*, 813–819.

40. Lin, C.-E.; Fang, L.-F. A novel positively charged nanofiltration membrane formed via simultaneous cross-linking/quaternization of poly(m-phenylene isophthalamide)/polyethyleneimine blend membrane. *Sep. Purif. Technol.* **2019**, *212*, 101–109.

41. Fang, L.-F.; Zhou, M.-Y. Positively charged nanofiltration membrane based on cross-linked polyvinyl chloride copolymer. *J. Memb. Sci.* **2019**, *572*, 28–37.

42. Zhai, Z.; Jiang, C. Fabrication of advanced nanofiltration membranes with nanostrand hybrid morphology mediated by ultrafast noria–polyethyleneimine codeposition. *J. Mater. Chem. A* **2018**, *6*, 21207–21215.

 doi:10.20944/preprints201911.0012.v2

43. Freger, V. Kinetics of film formation by interfacial polycondensation. *Langmuir* **2005**, *21*, 1884–1894.

44. Ohta, K.; Iwamoto, R. Experimental proof of the relation between thickness of the probed surface layer and absorbance in FT-IR/ATR spectroscopy. *Appl. Spectrosc.* **1985**, *39*, 418–425.

45. Singh, P. S.; Joshi, S. V. Probing the structural variations of thin film composite RO membranes obtained by coating polyamide over polysulfone membranes of different pore dimensions. *J. Memb. Sci.* **2006**, *278*, 19–25.